Biophysical Journal
Article

Biophysical Society

The Effect of Phosphatidylserine on a pH-Responsive Peptide Is Defined by Its Noninserting End

Vanessa P. Nguyen,[1] Andrew C. Dixson,[1] and Francisco N. Barrera[1,*]
[1]Department of Biochemistry & Cellular and Molecular Biology, University of Tennessee, Knoxville, Tennessee

ABSTRACT The acidity-triggered rational membrane (ATRAM) peptide was designed to target acidic diseases such as cancer. An acidic extracellular medium, such as that found in aggressive tumors, drives the protonation of the glutamic acids in ATRAM, leading to the membrane translocation of its C-terminus and the formation of a transmembrane helix. Compared to healthy cells, cancerous cells often increase exposure of the negatively charged phosphatidylserine (PS) on the outer leaflet of the plasma membrane. Here we use a reconstituted vesicle system to explore how PS influences the interaction of ATRAM with membranes. To explore this, we used two new variants of ATRAM, termed K2-ATRAM and Y-ATRAM, with small modifications at the noninserting N-terminus. We observed that the effect of PS on the membrane insertion p*K* and lipid partitioning hinged on the sequence of the noninserting end. Our data additionally indicate that the effect of PS on the insertion p*K* does not merely depend on electrostatics, but it is multifactorial. Here we show how small sequence changes can impact the interaction of a peptide with membranes of mixed lipid composition. These data illustrate how model studies using neutral bilayers, which do not mimic the negative charge found in the plasma membrane of cancer cells, may fail to capture important aspects of the interaction of anticancer peptides with tumor cells. This information can guide the design of therapeutic peptides that target the acidic environments of different diseased tissues.

SIGNIFICANCE Current targeted therapies for cancer have limited success due to drug resistance. Resistance often arises after mutation of the receptor being targeted. A more general target is needed to prevent drug resistance. Most aggressive solid tumors have an extracellular medium. We propose that extracellular acidity is promising for improved targeted therapies. The acidity-triggered rational membrane (ATRAM) peptide inserts in membranes only under acidic conditions. However, it is not known how the lipid changes that occur in the plasma membrane of cancer cells impact the membrane insertion of ATRAM. Here we perform biophysical experiments that show that phosphatidylserine, a lipid exposed in the cancer cell, can impact the membrane insertion of ATRAM. We also uncovered a region of the peptide important for insertion.

INTRODUCTION

Efficacious targeting of specific molecular markers in cancer is limited by tumor heterogeneity and drug resistance acquired due to rapid mutation (1). Therefore, it can be advantageous to target instead an intrinsic tumor property, such as extracellular acidity (2). Cancer cells preferentially metabolize glucose in the presence of oxygen due to the Warburg effect, resulting in increased secretion of lactic acid (3). Combined with poor tumor perfusion, this leads to the accumulation of acidic metabolites that reduce the pH of the extracellular matrix (4). We developed the acidity-triggered rational membrane (ATRAM) peptide to target the acidic extracellular environment of tumors (5). Biophysical and cellular experiments have shown that the membrane interaction of this highly soluble peptide is pH-dependent. At physiological pH, ATRAM partitions to lipid membranes, but at acidic pH it inserts into the membrane as an α-helix. ATRAM has been able to deliver a cell-impermeable toxin into HeLa cells as well as efficiently target solid tumors in mice (6). The insertion p*K* of ATRAM in POPC (1-palmitoyl-2-oleoyl-sn-glycero-3-phosphocholine)

Submitted April 30, 2019, and accepted for publication July 15, 2019.
*Correspondence: fbarrera@utk.edu
Editor: Arne Gericke.
https://doi.org/10.1016/j.bpj.2019.07.023

vesicles was previously determined to be 6.5 (5). This pH is at the lower limit of tumor extracellular acidity (7,8). To address the need to target mildly acidic tumors, here we worked to tune the tumor-targeting properties by designing two variants with N-terminal modifications. The effect of positively charged amino acids and aromatic amino acids on the insertion of ATRAM was studied.

Previous biophysical experiments studying the membrane interaction of ATRAM have been limited to POPC (5,6). However, the lipid bilayer of the plasma membrane is highly complex because both leaflets contain a variety of different lipids (9). A particularly important lipid is phosphatidylserine (PS). PS represents ~10% of the phospholipids in the plasma membrane and remains largely sequestered in the inner leaflet of healthy cells due to lipid asymmetry (10). However, cancerous cells can lose this asymmetry and as a result contain PS on both leaflets of their plasma membranes (11,12). Unlike PC lipids that contain a zwitterionic headgroup, PS is a net negatively charged phospholipid. ATRAM has a strong negative net charge at physiological pH; therefore, electrostatic repulsion may emerge between the negative charges of the peptide and the membrane of tumor cells, and control peptide-lipid interactions.

Here we show that the membrane insertion p*K* of ATRAM did not change with increasing PS concentrations, but how the peptide interacted with the membrane was altered. In contrast, in the N-terminal (N_t) variants, PS had a significant effect on membrane interaction and insertion. We investigated electrostatic interactions as a possible explanation for these different behaviors by performing additional experiments in the presence of NaCl. By understanding how negatively charged lipids affect the insertion of ATRAM into membranes, we can rationally fine-tune the sequence of ATRAM to increase its efficacy to insert into cancer cell membranes.

MATERIALS AND METHODS

Preparation of liposomes

Stocks of POPC and POPS (Avanti Polar Lipids, Alabaster, AL) were prepared in chloroform. Lipids were dried by flushing with argon gas and placed under a vacuum overnight. The resulting dried lipid films were hydrated with 10 mM sodium phosphate (pH 8.0) and extruded with a Mini-Extruder (Avanti Polar Lipids) through 100-nm polycarbonate filters (Whatman, Maidstone, United Kingdom) to create large unilamellar vesicles.

Peptide labeling

The C-terminal Cys of the ATRAM or K2-ATRAM variants (Table 1) was conjugated with the environmentally sensitive dye N, N′-dimethyl-N-(iodoacetyl)-N′-(7-nitrobenz-2-oxa-1,3-diazol-4-yl)ethylenediamine (NBD; Thermo Fisher Scientific, Waltham, MA). Y-ATRAM (Table 1) was labeled at the N-terminus with succinimidyl 6-n-7-nitrobenz-2-oxa-1,3-diazol-4-yl amino hexanoate (NBD-X SE; Anaspec, Fremont, CA). Free NBD dye was removed by gel filtration using a PD-10 column (GE Healthcare Life Sciences, Marlborough, MA), whereas labeled and unlabeled peptide were separated by reverse-phase HPLC (Agilent, Santa Clara, CA). The purity of the conjugations was confirmed by MALDI-TOF (Bruker, Billerica, MA).

pK_{FI} determination

Peptides were dissolved in 10 mM sodium phosphate pH 8.0 and incubated with lipid vesicles composed of POPC. After a 1-h incubation at room temperature, the samples were pH-corrected with 100 mM buffers (sodium acetate, 2-(N-morpholino)ethanesulfonic acid [MES], HEPES, or sodium phosphate). The final pH was measured after obtaining the fluorescence spectra. The molar lipid-to-peptide ratio was 200:1, with a final peptide concentration of 1 μM. The lipid-to-peptide ratio was changed to 150:1 for experiments studying the effect of salt due to the scattering effect of sodium chloride on the lipid vesicles. The final sodium chloride concentration in those experiments was 150 mM. Tryptophan fluorescence emission spectra were measured on a QuantaMaster fluorometer (Photon Technology International, Birmingham, NJ) with $\lambda_{ex} = 280$ nm and $\lambda_{em} = 310$–400 nm. The emission polarizer was set to 90°, and the excitation polarizer was set to 0° to reduce the light scattering effect of liposomes (13). Appropriate lipid backgrounds were subtracted in all cases. Fluorescence intensities at 335 nm (F) were fitted to determine the pK_{FI}, using:

$$F = \frac{F_a + F_b * 10^{m(pH - pK_{FI})}}{1 - 10^{m(pH - pK_{FI})}} \quad (1)$$

where F_a is the acidic baseline, F_b is the basic baseline, pK_{FI} is the midpoint of the sigmoidal curve, and m is the slope of the linear transition region between the baselines.

We then varied the composition of the lipid vesicles by gradually increasing the molar percent of PS (specifically, POPS) from 0 to 20%. The amount of PS needed to reach 50% of change in pK_{FI} was defined as PS_{50} and calculated according to:

$$pK = FI_o + (\Delta FI \times (x/(PS_{50} + x))) \quad (2)$$

where FI_o is the pK_{FI} at 0% PS, ΔFI is the change in the pK_{FI}, and x is the molar percentage of PS.

Circular dichroism

Peptides were prepared in 10 mM sodium phosphate pH 8.0 and incubated with POPC or POPC/POPS (1-palmitoyl-2-oleoyl-*sn*-glycero-3-phospho-*L*-serine; 9:1 molar ratio) vesicles. The pH of the samples

TABLE 1 Sequences of the ATRAM Peptide and Variants

Peptide	Sequence	Charge pH 4	Charge pH 8
ATRAM	GLAGLAGLLGL**E**GLLGLPLGLLEGL**W**LGLELE**G**N	0	−4
K2-ATRAM	G***K***AG***K***AGLLGL**E**GLLGLPLGLLEGL**W**LGLELE**G**N	+2	−2
Y-ATRAM	G***Y***AGLAGLLGL**E**GLLGLPLGLLEGL**W**LGLELEGN	0	−4

N-terminal modifications are shown in italics, and the single tryptophan and the key residue E12 are depicted in bold. Black G residues in bold are replaced with C for conjugation. Expected total side chain charge at acidic and basic pHs are shown.

was adjusted with 100 mM sodium acetate pH 4 or 100 mM sodium phosphate pH 8 after a 1-h incubation at room temperature. The final pH was measured after measuring the spectra. The lipid-to-peptide ratio was 200:1 with a final peptide concentration of 5 μM. Appropriate blanks were subtracted. Measurements were performed on a Jasco J-815 spectropolarimeter (Easton, MD) at room temperature. Raw data were transformed to mean residue ellipticity according to

$$[\Theta] = \frac{\Theta}{10lc(N-1)} \quad (3)$$

where Θ is the measured ellipticity in millidegree, l is the path length of the cuvette in cm, c is the peptide concentration in M, and N is the number of residues.

Oriented circular dichroism

Lipid or lipid-peptide (50:1 molar ratio) films were resuspended in methanol and added onto two circular quartz slides (Hellma Analytics, Müllheim, Germany). The slides were placed under vacuum for 24 h to evaporate the solvent. The samples on the slides were rehydrated with 100 mM sodium acetate pH 4 for 16 h at room temperature at 96% relative humidity. The slides with the samples were placed on opposite sides of the oriented circular dichroism (OCD) cell in a manner that would seal the cell. This ensured that the saturated K_2SO_4 that filled the inner cavity of the cell would remain hydrated and constantly humidify the sample throughout the experiment. The sample was recorded on a Jasco J-815 spectropolarimeter at room temperature. Eight 45° angle intervals were measured to prevent the artifacts caused by linear dichroism and then averaged for the final spectrum. Data were converted into mean residue ellipticity after lipid blanks were subtracted. The theoretical transmembrane (TM) and peripheral helix spectra was calculated as described by Wu et al. (14).

NBD lipid binding assay

NBD-labeled peptides were prepared in 10 mM sodium phosphate pH 8.0 and incubated with various POPC or POPC/POPS (9:1 molar ratio) concentrations at a final peptide concentration of 0.2 or 0.5 μM. The lipid-to-peptide ratios were maintained over the two peptide concentrations. After a 1-h incubation at room temperature, the pH of the samples was changed with 100 mM sodium acetate pH 4.05 or 100 mM sodium phosphate pH 7.5. Fluorescence spectra were measured on a Cytation 5 microplate reader (BioTek Instruments, Winooski, VT) with $\lambda_{ex} = 470$ nm and $\lambda_{em} = 520$–600 nm. Fluorescence intensities at 540 nm (F) were normalized to the highest value of each individual binding curve and were fitted with:

$$F = F_o + \Delta F \times \frac{K_p \times [L]}{55.3 + K_p \times [L]} \quad (4)$$

where F_o is the initial fluorescence intensity, ΔF is the overall change in fluorescence signal, K_p is the partition coefficient, [L] is the concentration of lipids, and 55.3 is the molar concentration of water.

Statistical analysis

Statistical analysis on pK_{FI} and K_p was performed using the SPSS v.25 software (IBM, Armonk, NY). Levene's test was performed to determine the homogeneity of the variance. Multiple comparisons tests were chosen based on the homoscedasticity (Tukey) or heteroscedasticity (Dunnett T3) of the data. Comparison of the pK_{FI} values was performed using the Tukey test, whereas the K_p was compared using the Dunnett T3 test. A value of $p \leq 0.05$ was considered significant. The n values presented in the figure legends refer to biological replicates consisting of independent repetitions of the full protocols.

RESULTS

ATRAM variants

The molecular basis of the interaction of ATRAM with lipid membranes is poorly understood. We performed mutational analysis to fill this void in knowledge. When ATRAM folds into the membrane forming a transmembrane (TM) helix, it does so inserting the C-terminal end (C_t) across the membrane (15). To avoid disrupting the overall membrane interaction of the peptide, we did not mutate the C_t. Instead, we modified the N_t to create two peptide variants, named K2-ATRAM and Y-ATRAM (Table 1). K2-ATRAM contains two positively charged lysines and allows studying the effect of the presence of positive charges because ATRAM only contains negatively charged residues. The single mutation in Y-ATRAM informs on the effect of hydrophobicity because the highly hydrophobic leucine was replaced by the mildly hydrophobic tyrosine residue.

We first performed studies at pH 8, where ATRAM binds to the membrane surface, and then at pH 4, which triggers ATRAM to adopt a TM orientation (5). Tryptophan fluorescence emission (Fig. 1) showed that the overall pH-responsiveness of the two new peptide variants was similar to ATRAM. This was the case in the presence of both POPC and POPC/POPS (molar ratio = 9:1) lipid vesicles. Specifically, we observed that upon a pH decrease, the fluorescence intensity increased, and the maximum of the spectra blue-shifted more than 10 nm (Fig. 1; Table 2). These results indicate that upon acidification the single W residue (Table 1) transitioned from a polar environment to a more hydrophobic medium. The CD spectra showed that at pH 8 all peptides were mostly unstructured, both in buffer and in lipid vesicles. As expected, they all formed α-helices in the presence of lipid vesicles at pH 4 (Fig. S1).

OCD was performed to study the helical orientation of the peptides with respect to the plane of the bilayer at acidic pH. An α-helix laying on top of a lipid bilayer generates an OCD spectrum with two clear minima at ~205 and ~222 nm. However, the OCD spectrum of a TM helix has a single broad minimum at ~225 nm. Our experimental data indicate that all peptides adopted a TM orientation at pH 4 in both lipid compositions (Figs. 2 and S2) with a small helical tilt. Theoretical OCD curves in POPC vesicles are shown along the measured curves of the peptides (Fig. 2). The variation between the theoretical curves of the different peptides arises from the fact that the theoretical curves depend on the fractional helicity of the peptides (14,16). Taken together, these studies demonstrate that the mutations do not hamper pH-dependent membrane insertion.

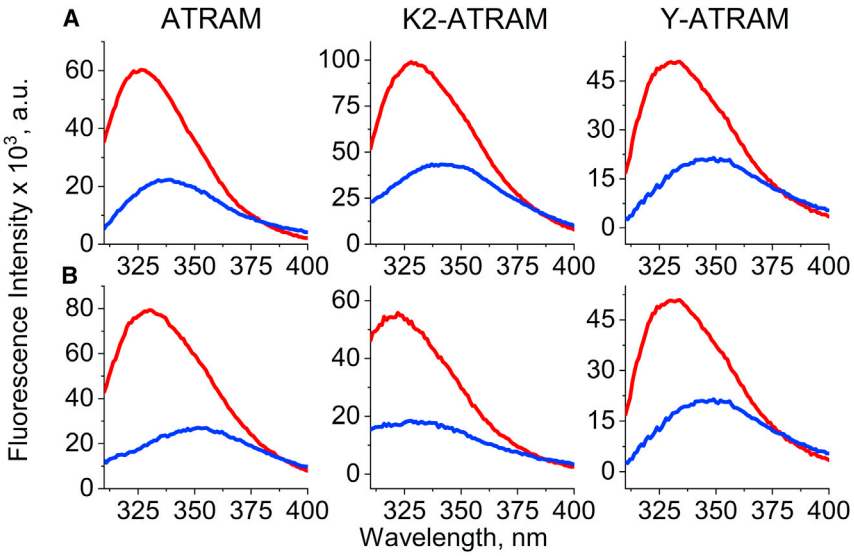

FIGURE 1 ATRAM, K2-ATRAM, and Y-ATRAM interact with the lipid membrane in a pH-dependent manner. Representative intrinsic tryptophan fluorescence spectra in the presence of POPC (*A*) and POPC/POPS (9/1) (*B*) vesicles at pH 4 (*red*) and pH 8 (*blue*). To see this figure in color, go online.

p*K* of membrane insertion

To determine the pH midpoint of the membrane insertion of the peptides, we followed the changes of the tryptophan fluorescence intensities as the pH decreased from pH ~8 to pH ~4 (Fig. 3). The pH midpoint of this sigmoidal titration is defined as the pK_{FI} (17). In all cases, we observed that acidification caused sigmoidal fluorescence changes. In experiments performed with POPC vesicles, the pK_{FI} of ATRAM (6.20 ± 0.15) was similar to that of Y-ATRAM (6.27 ± 0.12). However, for K2-ATRAM, we observed a large acidic shift, resulting in a pK_{FI} of 5.42 ± 0.14.

We studied if similar results were observed when PS was present in the vesicles. To this end we repeated the pH titrations with seven PS levels between 0 and 20%, to cover the physiologically relevant range (18). Intriguingly, we observed that the impact of PS in the pK_{FI} was markedly different between the three peptides (Figs. 4 *A* and S3). The pK_{FI} of ATRAM was not significantly affected by the presence of PS in the lipid vesicles. However, there was a different, and opposite, behavior for K2-ATRAM and Y-ATRAM. Thus, PS caused a ~0.4 pH units increase in the pK_{FI} for K2-ATRAM. However, PS caused a decrease in the pK_{FI} for Y-ATRAM (~0.3 pH units). The PS changes were hyperbolic, and fitting to Eq. 2 allowed determining the PS midpoint (PS_{50}). The PS_{50} values were 1.9% PS for K2-ATRAM, and 0.5% PS for Y-ATRAM. These low values illustrate that the effect on the pK_{FI} occurred at low concentrations of PS, well within those present in most eukaryotic cells (18).

TABLE 2 Fluorescence Spectral Maxima (nm) at Acidic and Basic pH Values

	ATRAM	K-ATRAM	Y-ATRAM
POPC acidic	327.3 ± 0.7	329.7 ± 1.2	324.5 ± 2.9
POPC basic	341.1 ± 2.3	342.1 ± 2.1	343.9 ± 3.6
POPC/POPS acidic	330.8 ± 0.8	320.2 ± 1.7	320.5 ± 1.9
POPC/POPS basic	350.9 ± 1.0	331.7 ± 1.8	342.7 ± 2.3

The effect of PS on the pK_{FI} of Y-ATRAM is similar to the effect we had previously reported with pHLIP, a different pH-sensitive membrane peptide (19). For pHLIP, the pK_{FI} decrease was due to electrostatic repulsion between the negative charges in PS and pHLIP, which was screened in the presence of NaCl. To study whether electrostatics also controlled the membrane insertion of the three ATRAM peptides, the pK_{FI} was also determined in the presence of 150 mM NaCl (Figs. 4 *B* and S3). For ATRAM, the pK_{FI} of both lipid conditions decreased compared to the values obtained in the absence of NaCl. Similarly, a pK_{FI} decrease was observed for Y-ATRAM for both lipid compositions. In the presence of NaCl both peptides showed similar pK_{FI} in POPC and POPC/POPS.

A more nuanced scenario was observed for K2-ATRAM because NaCl decreased pK_{FI} only in POPC/POPS but not for POPC liposomes (Fig. 4 *B*). Again, the difference in pK_{FI} between POPC and POPC/POPS vesicles was lost in the presence of NaCl. An additional feature of K2-ATRAM is that the pK_{FI} in the presence of NaCl (~5.4) was lower than for ATRAM and Y-ATRAM, with a value in both cases of ~5.7. These results indicate that fundamental differences exist in how K2-ATRAM and the two other peptides interact with lipid membranes. Due to lipid light scattering, titrations in the presence of NaCl were performed with a lipid-to-peptide ratio of 150:1 instead of 200:1. We performed control experiments that showed that in the presence of 150 mM NaCl there were no significant differences in the pK_{FI} of ATRAM at 150:1 and 200:1 POPC-to-peptide ratios, (Fig. S4). To unravel the causes for the different effect of PS on the three ATRAM peptides, we performed additional studies.

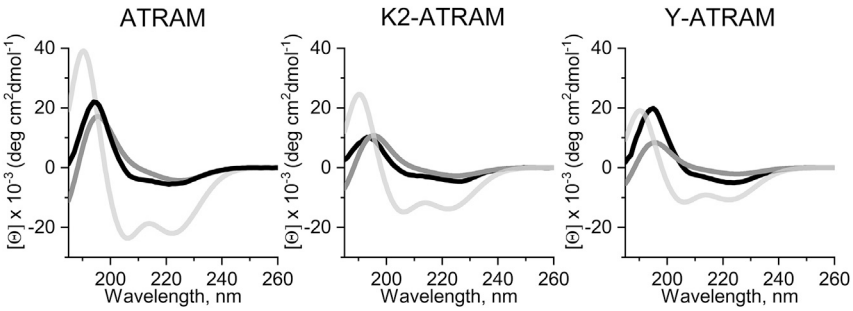

FIGURE 2 All peptides adopt a TM conformation at acidic pH. OCD spectra of the peptides (*black*) in hydrated stacked POPC bilayers. The gray lines correspond to theoretical spectra for a TM (*dark gray*) and surface-bound (*light gray*) α-helix.

Partition coefficient

We have previously reported that the POPC affinity of ATRAM is higher at acidic pH than neutral pH as a consequence of the increased hydrophobicity resulting from the protonation of glutamic acids (15). We obtained similar results for all ATRAM variants in POPC (Fig. 5). Interestingly, at acidic pH, the effect of POPS on the partition coefficient mirrors the trends seen in the pK_{FI} (Fig. 4 *B*). Thus, at pH 4, the presence of POPS did not affect the K_p for ATRAM (Fig. 5), but it increased for K2-ATRAM (as it increased pK_{FI}) and decreased for Y-ATRAM (as it decreased pK_{FI}). Previously, the binding of ATRAM to the lipid membrane was considered nonideal because the partition coefficient depended on the peptide concentration, and thus the K_p we report is in reality an apparent K_p (15). Here we show that this was also true for all the variants in both lipid composition because when we repeated the binding assay at a lower peptide concentration, the K_p values were significantly higher (Figs. S5 and S6). However, similar trends were observed in both cases.

DISCUSSION

PS is the most abundant negatively charged lipid in the plasma membrane of eukaryotic cells (18). PS plays multiple regulatory roles on membrane proteins, that result in changes in activity (20), polymerization (21), and clustering (22), as well as driving membrane interaction of soluble peripheral membrane proteins (23) and myristoylated proteins (24). PS is distributed asymmetrically in the plasma membrane of human cells, with high levels in the cytoplasmic leaflet, and low levels present in the extracellular leaflet (25,26). PS asymmetry, however, can be lost in cancer cells, where PS is increasingly exposed at the cell surface (11,27,28). This provides the opportunity of targeting PS to direct selective drug delivery to cancer cells.

In this work, we studied the effect on ATRAM of the presence of POPS in the membrane. We designed two new ATRAM variants to study the effect of the properties of the peptide N_t. Fluorescence and circular dichroism confirmed that the variants maintained pH-sensitive properties. Despite the observation that PS affects the interaction of the bilayer with the peptides, those changes appear subtle because they do not involve large changes in secondary structure (Fig. 2). Furthermore, OCD experiments in POPC showed that all peptides acquired a TM conformation at low pH. The similarity in the OCD spectra in this lipid indicates that all variants adopt a similar tilt angle in the membrane. The OCD spectra of the peptides in POPC/POPS had a lower signal than those in POPC (Fig. S2). A possible explanation is that that the negative charges of PS caused bilayer repulsion (29), making it harder for lipid bilayers to stack on top of each other on the quartz slide, artifactually reducing the overall signal.

We determined that the pK_{FI} of ATRAM in POPC vesicles was 6.2. However, the previously published insertion pK value of ATRAM in POPC was 6.5 (5). This latter value was determined by following the shift of the fluorescence spectral maximum over a pH range, whereas the new value

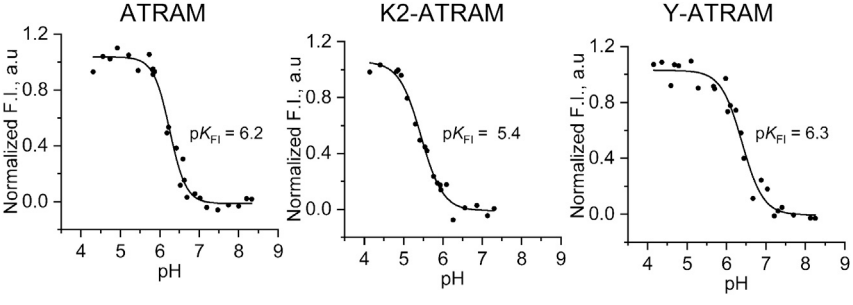

FIGURE 3 Representative pH titration curves of ATRAM and the two variants. The pK_{FI} of each peptide in POPC was determined as the midpoint of the change in the peptide intrinsic fluorescence intensities, obtained by fitting to Eq. 1. Values of pK_{FI} are shown for each panel.

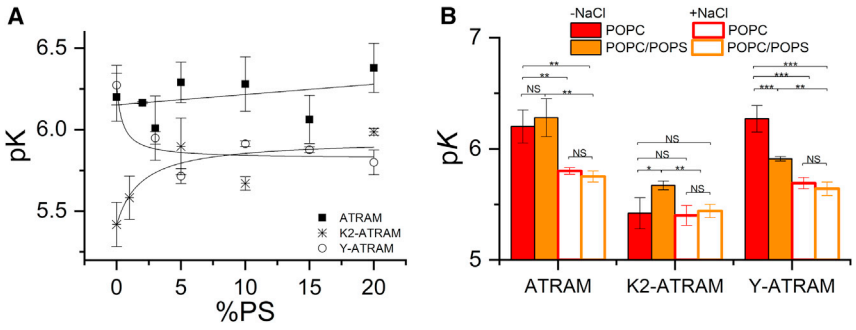

FIGURE 4 The effect of POPS and NaCl on the pK_{FI}. (*A*) Increasing levels of PS effect on ATRAM (*squares*), Y-ATRAM (*circles*), and K2-ATRAM (*stars*). (*B*) Effect of the addition of 150 mM NaCl on the pK_{FI} in POPC or POPC/POPS (9/1). Mean pK_{FI} values from (*A*) plus additional data obtained in the presence of NaCl are shown ± S.D. $n = 3$–6, $*p < 0.05$, $**p < 0.01$, $***p < 0.001$, NS, no significance. To see this figure in color, go online.

was determined by following instead changes in intensity. It has previously been shown for the pHLIP peptide that different methods of spectral analysis result in changes in p*K* values because each method reported different membrane insertion intermediates (17). Previous stopped-flow fluorescence data showed that ATRAM populates at least three intermediates when transitioning from the peripheral state to the TM conformation (15). This result suggests that the observed differences in p*K* values of ATRAM might be associated with the preferential detection of different conformational intermediates.

In POPC vesicles, we observed a decreased pK_{FI} for K2-ATRAM compared to ATRAM and Y-ATRAM (Fig. 4). This result indicates that the addition of the two basic residues resulted in more protons being required for the peptide to insert. Studies in the presence of NaCl revealed that ATRAM and Y-ATRAM electrostatically interact with POPC, but this was not the case with K2-ATRAM because there was no change in pK_{FI} with the addition of NaCl. As tumor cells expose PS on the outer leaflet of their cell membranes (30), we studied the effect of PS on the membrane interaction of the peptides. Although PS did not affect the pK_{FI} of ATRAM, it affected the two variants in an opposite fashion. For K2-ATRAM, the observed increase in pK_{FI} is expected to result from favorable interactions with the negative charge of PS. As with ATRAM and Y-ATRAM, the addition of NaCl resulted in a decrease in pK_{FI} for K2-ATRAM, indicating that the interaction with PS has an electrostatic component for all peptides. The NaCl experiments were also performed at a lower lipid-to-peptide ratio (150:1 vs. 200:1). Although the pK_{FI} did not differ for these two ratios (Fig. S4), we cannot totally rule out that the fluorescence data for Y-ATRAM is influenced by the presence of peptide in solution as a result from working at nonsaturating conditions at pH 7.5 (Fig. S6). This effect is likely a result from the Leu to Tyr mutation decreasing peptide hydrophobicity. However, we expect this effect not to be large because a pH decrease increases the membrane affinity and thus the fraction of membrane-bound peptides (Fig. 5).

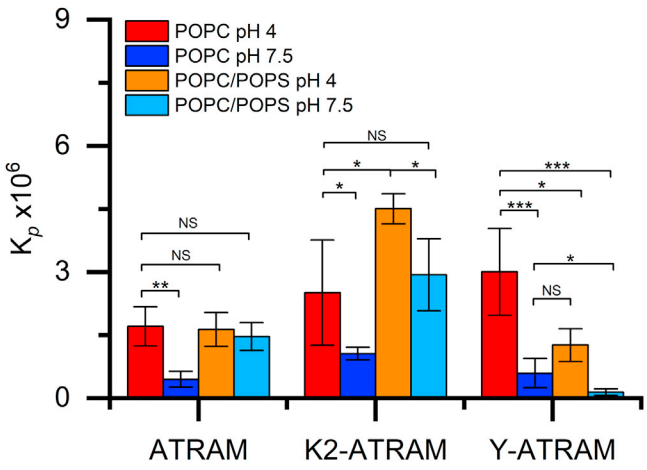

FIGURE 5 Apparent K_p of ATRAM peptides in POPC and POPC/POPS (9/1). Mean values are shown ± S.D. $n = 3$–4, $*p < 0.05$, $**p < 0.01$, $***p < 0.001$, NS, no significance. To see this figure in color, go online.

The complexity in the effect of PS and NaCl on the peptides suggests that the interaction is not controlled by a simple electrostatic process (19). For pHLIP, it is proposed that the decrease in membrane insertion p*K* caused by PS results from the protonatable residues being more hydrated (19). This would result from the peptide having a shallower position on the membrane surface due to the presence of negatively charged lipids. As a result, there would be enhanced exposition to the aqueous environment of the side chains of the protonatable (Asp and Glu) residues. The spectral maximum of the C_t Trp is sensitive to hydration and thus reports the degree of membrane embedding, with a lower spectral maximum indicating deeper insertion into the hydrophobic bilayer (Table 2). In ATRAM, the single Trp is surrounded by three of the four Glu residues. However, we did not observe a good correlation between the Trp hydration and the pK_{FI}. Then, we hypothesize that the remaining Glu residue, away from the Trp at position 12 (E12), controls the insertion pK_{FI} changes.

Integration of the data of Table 2 and Fig. 4 *A* allows us to propose a working model for the interaction of the peptides with the surface of the membrane (Fig. 6). In ATRAM, the residues W26 and E12 are similarly immersed on the lipid polar headgroup both in POPC and POPC/POPS vesicles, resulting in a similar pK_{FI}. In K2-ATRAM, in POPC the N_t, including E12, is away from the membrane, resulting

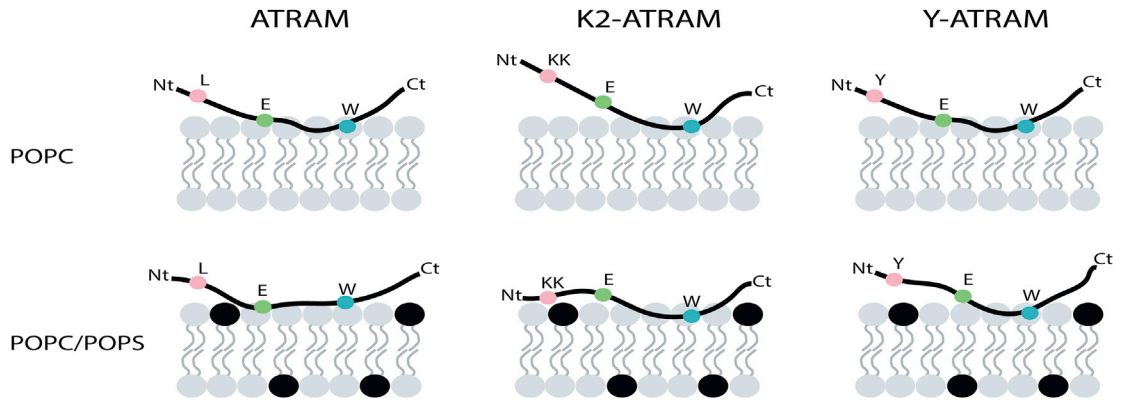

FIGURE 6 Schematic of the surface-bound state of the ATRAM peptides. The proposed locations of E12 and W26 residues are shown in green and blue, respectively, whereas the modified residues at the N-terminal are marked in pink. The two lysines are represented as a single sphere. The headgroup of PS is highlighted in black. To see this figure in color, go online.

in a lower pK_{FI}, which is closer to ~4.0–4.5, the value typically observed for Glu in solution (31). However, when POPS is present in the membrane, an attractive interaction occurs between the negative charges of PS and the positively charged lysines. As a result, the N_t approaches the membrane, altering the polarity of the environment of E12 to increase the pK of this residue. In the case of Y-ATRAM, the cause of the effect of PS on the pK_{FI} is less clear. However, we hypothesize an involvement of the polar nature of the Tyr ring, which provides a surface of negative electrostatic potential that could cause electrostatic repulsion with the PS headgroup (32). As a result, E12 would more exposed to the aqueous environment, which is expected to decrease the insertion pK_{FI} in the presence of PS. Fig. 6 only shows the surface-bound state, as we propose that the TM state is similar in all cases.

ATRAM shows several differences compared with other soluble peptides that interact with membranes. Although ATRAM has a strong negative charge at neutral pH (Table 1), antimicrobial peptides (AMPs) and cell penetrating peptides (CPPs) contain multiple positive charges. When AMPs bind to cellular membranes, they disrupt the integrity of the bilayer, often by the formation of a membrane pore (33). On the other hand, CPPs translocate completely across the plasma membrane to interact with intracellular targets (34), whereas ATRAM is believed to target only the plasma membrane and not form pores (5). Additionally, the membrane interaction of AMPs and CPPs is promoted by their interaction with negatively charged lipids due to electrostatic attraction (35). As a result, they typically have a higher affinity toward anionic lipids like PS (36). Surprisingly, for ATRAM and K2-ATRAM at pH 7.5, we also observed higher membrane affinity in the presence of PS.

We observed a correlation between the membrane affinity at neutral pH (Fig. 5, K_p) and the pH-responsiveness of insertion (Fig. 4, pK_{FI}). The increase in affinity in the presence of POPS observed in K2-ATRAM was probably due to favorable electrostatic interactions of the positively charged Lys and the negatively charged PS, whereas the opposite was observed with Y-ATRAM. This highlights the importance of considering the equilibrium between surface-bound and soluble states for peripherally binding peptides and proteins. Determination of the K_p was carried out monitoring changes in the intensity of the NBD fluorophore. The NBD in Y-ATRAM was located at an opposite side of the membrane than the other two peptides. Although it is possible that this might change the fluorescence intensity, this is not expected to alter the K_p, which is not a parameter affected by the absolute intensity value (Eq. 4).

This work shows that the sequence opposite the inserting end can control the insertion of a membrane peptide. This indicates that for ATRAM, as well as for similar peptides such as TYPE7 (37) and pHLIP (38), the N_t is a promising region for modifications that improve tissue targeting or pharmacokinetics. In our case, the pK of insertion of the three peptides still remained more acidic than the pH of the extracellular matrix of tumor cells (pH 6.4–7.0) (2,39). However, it is important to consider that the local pH at the membrane surface is significantly more acidic than the bulk microenvironment pH (40,41). This suggests that the pH-triggered membrane insertion of ATRAM peptides could provide specificity for tumor targeting. Indeed, it has been recently reported that ATRAM efficiently targets tumors and is able to translocate drug-like molecules across the plasma membrane of cancer cells (6). Our results point toward the intriguing possibility that the exposure of PS in cancer cells could be used as an additional source of tumor specificity (42). Indeed, for K2-ATRAM, the presence of small amounts of PS rapidly increases the pK_{FI}, which is expected to increase cancer cell targeting. This might be the basis for K2-ATRAM potentially displaying an increased specificity for tumor cells. The opposite would be expected for the Y-ATRAM variant. We propose that our findings can be used to achieve improved design of peptides that target the membrane of cancer cells, particularly in the more acidic aggressive solid tumors.

SUPPORTING MATERIAL

Supporting Material can be found online at https://doi.org/10.1016/j.bpj.2019.07.023.

AUTHOR CONTRIBUTIONS

V.P.N. and A.C.D. performed the research. V.P.N., A.C.D., and F.N.B. designed the research and analyzed the data. V.P.N. and F.N.B. wrote the manuscript.

ACKNOWLEDGMENTS

We are thankful to Justin M. Westerfield and Yujie Ye for insightful comments on the manuscript. This work was supported by National Institutes of Health grant R01GM120642 to F.N.B.

REFERENCES

1. Janku, F. 2014. Tumor heterogeneity in the clinic: is it a real problem? *Ther. Adv. Med. Oncol.* 6:43–51.
2. Hao, G., Z. P. Xu, and L. Li. 2018. Manipulating extracellular tumour pH: an effective target for cancer therapy. *RSC Adv.* 8:22182–22192.
3. Griffiths, J. R. 1991. Are cancer cells acidic? *Br. J. Cancer.* 64:425–427.
4. Gillies, R. J., N. Raghunand, …, R. A. Gatenby. 2004. pH imaging. A review of pH measurement methods and applications in cancers. *IEEE Eng. Med. Biol. Mag.* 23:57–64.
5. Nguyen, V. P., D. S. Alves, …, F. N. Barrera. 2015. A novel soluble peptide with pH-responsive membrane insertion. *Biochemistry.* 54:6567–6575.
6. Wyatt, L. C., A. Moshnikova, …, Y. K. Reshetnyak. 2018. Peptides of pHLIP family for targeted intracellular and extracellular delivery of cargo molecules to tumors. *Proc. Natl. Acad. Sci. USA.* 115:E2811–E2818.
7. Gatenby, R. A., and R. J. Gillies. 2004. Why do cancers have high aerobic glycolysis? *Nat. Rev. Cancer.* 4:891–899.
8. Lacroix, R., E. A. Rozeman, …, C. U. Blank. 2018. Targeting tumor-associated acidity in cancer immunotherapy. *Cancer Immunol. Immunother.* 67:1331–1348.
9. van Meer, G., and A. I. de Kroon. 2011. Lipid map of the mammalian cell. *J. Cell Sci.* 124:5–8.
10. Bretscher, M. S., and M. C. Raff. 1975. Mammalian plasma membranes. *Nature.* 258:43–49.
11. Utsugi, T., A. J. Schroit, …, I. J. Fidler. 1991. Elevated expression of phosphatidylserine in the outer membrane leaflet of human tumor cells and recognition by activated human blood monocytes. *Cancer Res.* 51:3062–3066.
12. Bretscher, M. S. 1972. Asymmetrical lipid bilayer structure for biological membranes. *Nat. New Biol.* 236:11–12.
13. Ladokhin, A. S., S. Jayasinghe, and S. H. White. 2000. How to measure and analyze tryptophan fluorescence in membranes properly, and why bother? *Anal. Biochem.* 285:235–245.
14. Wu, Y., H. W. Huang, and G. A. Olah. 1990. Method of oriented circular dichroism. *Biophys. J.* 57:797–806.
15. Nguyen, V. P., L. Palanikumar, …, F. N. Barrera. 2019. Mechanistic insights into the pH-dependent membrane peptide ATRAM. *J. Control. Release.* 298:142–153.
16. Usery, R. D., T. A. Enoki, …, G. W. Feigenson. 2018. Membrane bending moduli of coexisting liquid phases containing transmembrane peptide. *Biophys. J.* 114:2152–2164.
17. Scott, H. L., J. M. Westerfield, and F. N. Barrera. 2017. Determination of the membrane translocation pK of the pH-low insertion peptide. *Biophys. J.* 113:869–879.
18. van Meer, G., D. R. Voelker, and G. W. Feigenson. 2008. Membrane lipids: where they are and how they behave. *Nat. Rev. Mol. Cell Biol.* 9:112–124.
19. Scott, H. L., V. P. Nguyen, …, F. N. Barrera. 2015. The negative charge of the membrane has opposite effects on the membrane entry and exit of pH-low insertion peptide. *Biochemistry.* 54:1709–1712.
20. Alvis, S. J., I. M. Williamson, …, A. G. Lee. 2003. Interactions of anionic phospholipids and phosphatidylethanolamine with the potassium channel KcsA. *Biophys. J.* 85:3828–3838.
21. Barrera, F. N., M. del Alamo, …, J. L. Neira. 2008. Envelope lipids regulate the in vitro assembly of the HIV-1 capsid. *Biophys. J.* 94:L8–L10.
22. Platre, M. P., V. Bayle, …, Y. Jaillais. 2019. Developmental control of plant Rho GTPase nano-organization by the lipid phosphatidylserine. *Science.* 364:57–62.
23. Köhler, G., U. Hering, …, K. Arnold. 1997. Annexin V interaction with phosphatidylserine-containing vesicles at low and neutral pH. *Biochemistry.* 36:8189–8194.
24. Sigal, C. T., W. Zhou, …, M. D. Resh. 1994. Amino-terminal basic residues of Src mediate membrane binding through electrostatic interaction with acidic phospholipids. *Proc. Natl. Acad. Sci. USA.* 91:12253–12257.
25. Balasubramanian, K., and A. J. Schroit. 2003. Aminophospholipid asymmetry: a matter of life and death. *Annu. Rev. Physiol.* 65:701–734.
26. van Meer, G. 2011. Dynamic transbilayer lipid asymmetry. *Cold Spring Harb. Perspect. Biol.* 3:a004671.
27. Ran, S., A. Downes, and P. E. Thorpe. 2002. Increased exposure of anionic phospholipids on the surface of tumor blood vessels. *Cancer Res.* 62:6132–6140.
28. Riedl, S., B. Rinner, …, D. Zweytick. 2011. In search of a novel target - phosphatidylserine exposed by non-apoptotic tumor cells and metastases of malignancies with poor treatment efficacy. *Biochim. Biophys. Acta.* 1808:2638–2645.
29. Nordlund, T. M., and P. M. Hoffmann. 2011. Two-dimensional aggregates: membranes. *In* Quantitative Understanding of Biosystems: An Introduction to Biophysics. CRC Press, pp. 158–168.
30. Zwaal, R. F., P. Comfurius, and E. M. Bevers. 2005. Surface exposure of phosphatidylserine in pathological cells. *Cell. Mol. Life Sci.* 62:971–988.
31. Castañeda, C. A., C. A. Fitch, …, B. E. García-Moreno. 2009. Molecular determinants of the pKa values of Asp and Glu residues in staphylococcal nuclease. *Proteins.* 77:570–588.
32. Dougherty, D. A. 2007. Cation-π interactions involving aromatic amino acids. *J. Nutr.* 137 (*Suppl 1*):1504S–1508S, discussion 1516S–1517S.
33. Hoskin, D. W., and A. Ramamoorthy. 2008. Studies on anticancer activities of antimicrobial peptides. *Biochim. Biophys. Acta.* 1778:357–375.
34. Di Pisa, M., G. Chassaing, and J. M. Swiecicki. 2015. Translocation mechanism(s) of cell-penetrating peptides: biophysical studies using artificial membrane bilayers. *Biochemistry.* 54:194–207.
35. Gaspar, D., A. S. Veiga, and M. A. Castanho. 2013. From antimicrobial to anticancer peptides. A review. *Front. Microbiol.* 4:294.
36. Mason, A. J., A. Martinez, …, B. Bechinger. 2006. The antibiotic and DNA-transfecting peptide LAH4 selectively associates with, and disorders, anionic lipids in mixed membranes. *FASEB J.* 20:320–322.
37. Alves, D. S., J. M. Westerfield, …, F. N. Barrera. 2018. A novel pH-dependent membrane peptide that binds to EphA2 and inhibits cell migration. *eLife.* 7.
38. Deacon, J. C., D. M. Engelman, and F. N. Barrera. 2015. Targeting acidity in diseased tissues: mechanism and applications of the

membrane-inserting peptide, pHLIP. *Arch. Biochem. Biophys.* 565:40–48.

39. Kato, Y., S. Ozawa, …, Y. Baba. 2013. Acidic extracellular microenvironment and cancer. *Cancer Cell Int.* 13:89.

40. Anderson, M., A. Moshnikova, …, O. A. Andreev. 2016. Probe for the measurement of cell surface pH in vivo and ex vivo. *Proc. Natl. Acad. Sci. USA.* 113:8177–8181.

41. Xu, M., X. Ma, …, B. Ren. 2018. In situ imaging of live-cell extracellular pH during cell apoptosis with surface-enhanced Raman spectroscopy. *Anal. Chem.* 90:13922–13928.

42. Mangoni, M. L., and Y. Shai. 2011. Short native antimicrobial peptides and engineered ultrashort lipopeptides: similarities and differences in cell specificities and modes of action. *Cell. Mol. Life Sci.* 68:2267–2280.